Reliability Engineering and System Safety 251 (2024) 110326

Contents lists available at ScienceDirect

Reliability Engineering and System Safety

journal homepage: www.elsevier.com/locate/ress

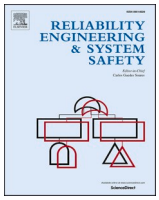

Performance-based multi-hazard engineering (PB-MH-E): The case of steel buildings under earthquake and wind

M. Francioli , F. Petrini *

Sapienza University of Rome, Rome, Italy

ARTICLE INFO

Keywords:
Multi-hazard
Wind
Earthquake
Performance-based design

ABSTRACT

Focusing on natural hazards as wind and earthquake, the goal of this work is to understand if interference occurs in the design choices for steel buildings of a certain height, thus determining which design requirement and hazard is predominant, between Ultimate Limit State (ULS) requirements under earthquakes, or comfort of the occupants and the Serviceability Limit State (SLS) of the structure under wind. Thus, in order to compare structural responses, both in linear (i.e., SLSs) and non-linear field (i.e., ULS) a simplified analysis procedure that could be also implemented in Standards and in design practice (so-called SAC-FEMA method, originally introduced in the seismic field by Cornell in the early 2000s and more recently extended to the wind) is adapted, leading to a true optimal Performance-Based Multi-Hazard Design (PB-MH-D) of the structure considering the two hazards. The procedure is applied to two case-study steel buildings, 17 and 60 floor heigh; the approach is shown to efficiently lead to a design solution who consistently tackles with the same level of reliability with the two hazards.

1. Introduction

As a follow-up to the events at the dawn of the new millennium related to Multi – Hazard (MH) scenarios striking on structures and infrastructures (e.g., 2005 hurricane Katrina or 2011 Tohoku earthquake in Japan), the need for approaches accounting for MH exposures in the structural design [1] has been clearly recognised by the scientific community, and, thanks to a worldwide policy for infrastructural management which supports the actions of the Sendai Framework for Disaster Risk Reduction 2015–30 [2], political efforts are ongoing in this direction. Despite this evidence, a methodology for the true MH design of structures who allows the performance evaluation under different threats in a coherent and uniform manner is still not available. Current structural design methods [3] tend to design the structures for ultimate limit states (ULSs) and serviceability limit states (SLSs) performances under the hazard that is supposed to be dominant for the specific LS, and then check the performances under other hazards separately, with the purpose of updating the design if required. This way of approaching the design cannot be considered a MH one, but rather a hazard-by-hazard approach, and it leads to a final solution which is not a global optimum (i.e., eligible as the best design configuration by considering both SLSs and ULSs for all the acting hazards), but it is rather a local one (mostly driven by one hazard and judged as acceptable for other hazards).

The traditional hazard-by-hazard design approaches have shown their ineffectiveness in some particular situations where neglecting hazard interactions can lead to serious underestimation of damage/losses. MH load scenarios involving Civil Engineering structures can be intended as consequences to natural and/or to man-made hazards [4,5]. The hazards can occur independently, simultaneously (as correlated each other) [6,7] or in concatenated chain scenarios ([8,9,10]), and interactions can arise either at action level, at the structural vulnerability level, or at the design indications level [11,12]. An example of interaction at the structural vulnerability level between chained hazard, is where a first action (e.g., due to an earthquake) strikes the structure followed by a second action (maybe triggered by the previous one, e.g., blast or fire after earthquake) [13], which impacts on a structure that, due to the damage induced by the first hazard, exhibits an increased vulnerability to the second one. A typical example of interaction at the design indications level between independent hazards occurs in structures that are equally sensitive to the different hazards (e.g., low-damped medium-rise buildings subjected to earthquake and wind) in which given certain design configurations, some opposite/competitive design indications can arise (e.g., increase flexibility to comply with

* Corresponding author.
E-mail addresses: mattia.francioli@uniroma1.it (M. Francioli), francesco.petrini@uniroma1.it (F. Petrini).

https://doi.org/10.1016/j.ress.2024.110326
Received 30 November 2023; Received in revised form 17 May 2024; Accepted 4 July 2024
Available online 10 July 2024

seismic performance requirements or increase stiffness to comply with wind performance requirements) [14]. The definition of design approaches that allows to properly consider such MH scenarios is a matter of urgency ([15,16]), especially for structures of particular importance, such as bridges, skyscrapers or hospitals, whose unsatisfactory performances can lead to significant social and economic impacts.

However, when the structural design deals with MH scenarios, many additional issues emerge with respect to those commonly tackled during the hazard-by-hazard design procedures; in particular, the methodological approaches and computational tools used in different fields (analysis under different hazards) need to be combined within a unified risk assessment/design framework (unified framework problem) [17], and in order to define such unified framework, the structural performances under different hazards must be expressed in an universal format where same performance indicators should be used for different hazards, and uncertainties affecting the capacities (C) and the demands (D) should be represented by the same models for different hazards. Valid candidates as universal performances indicators are the monetary losses potentially occurring in a reference period, or the structural risk (i.e., occurrence) related to ULSs or SLSs [18], while strong candidate models for C and D uncertainties are lognormal distributions [19,20].

This paper proposes such a framework for the above-mentioned design case of medium-rise, low-damped steel buildings under earthquake and winds. The framework is based on the so-called SAC-FEMA approach, originally developed and improved in years for performance-based earthquake engineering (PBEE) [19], and recently extended by the same authors of this paper to the performance-based wind engineering (PBWE) [21]. The SAC-FEMA approach allows for the evaluation of the mean annual frequency (MAF) for a certain limit state to occur. By considering in parallel the structural reliability against both earthquake-induced and wind-induced LSs, appropriate design choices are put in place to reach the desired and comparable reliability levels against both hazards by searching the design configuration characterized by MAFs that are as nearest as possible to the design acceptable occurrences for all LSs and for all involved hazards. In other words, the procedure leads to an optimal risk-based design configuration of the structures considering the two hazards.

The proposed framework is a novelty in the PB-MH-E literature since different hazards effects driving the design are taken into account by applying single-hazard focused procedures, often affected by different kind of uncertainties. Having a unified procedure, characterized by the same kind of variables and uncertainties characterization for the hazard, is something new.

It is worth that in case of wind and earthquake, the MH aspects do not focus on the simultaneous occurrence of the two hazards (which is known to be characterized by a very low probability), but rather on the correct design choices, which need to be balanced among conflicting design strategies highlighted by the two hazards. In this sense, the previous development of the SAC-FEMA WIND (which uses same performance metrics and performance evaluation tools of the SAC-FEMA for earthquakes) from the authors has been pursued to represent a first step toward the development of a true Performance-Based Multi-Hazard Engineering (PB-MH-E), while this paper represents the second step in the same direction by showing the first application of SAC-FEMA like methods to a MH case. The conceptualization of the analysis method proposed in this paper, regarding the possibility to assess at the same time the structural performances towards wind and earthquake, represents a novelty and leads to a general approach for PB-MH-E in case of concurrent independent hazard, which represents the main objective of this work.

2. Methods

2.1. Performance based multi – hazard engineering (PB-MH-E) and SAC-FEMA method

Performance-Based Engineering (PBE) is a widespread probabilistic design methodology whose main features, such as the possibility to explicitly define the performances that the structure must maintain during its life, the possibility to choose design methods that allow the structure to achieve such goals and to include innovative solutions, have ensured its application in different fields of civil engineering [16].

With specific reference to wind and earthquake, the performances of steel high rise frame-building under multiple hazards are assessed in this work using the SAC-FEMA probabilistic analysis method, since these two hazards are characterized by well-defined statistics. This performance-based-like approach provides the possibility to determine the Mean Annual Frequency (MAF) of a certain Limit State (LS) using a simplified algebraic formulation, avoiding the complexity of the traditional integral expression; this simplification is made possible through appropriate assumptions which concerns both the demand and the capacity definition. In particular, it is assumed that:

- the hazard curve is approximated by a second-order logarithmic interpolating law (in the case of "2nd order" improved SAC-FEMA formulation proposed by Vamvatsikos (2014) [22])

$$H(im) = k_{0,i,k}\ exp\left(- k_{2,i,k} ln^2(im) - k_{1,i,k} \ln(im)\right) \tag{1}$$

where $k_{0,i,k}$, $k_{1,i,k}$ and $k_{2,i,k}$ are constant coefficients, while im represents the sample scalar value of the Intensity Measure (IM) of the considered hazard;

- both C and D are assumed to follow lognormal distributions with median values and $\widehat{C}$ and $\widehat{D}$ and dispersions β_C and $\beta_{D|im}$ and β_C, being the D dispersion conditional to the IM value im. Namely $D \sim LN(\widehat{D}, \beta_{D|im})$ and $C \sim LN(\widehat{C}, \beta_C)$;

the median D value is approximated by a power interpolating function

$$\widehat{D} = a_{i,k} \cdot (im)^{b_{i,k}} \tag{2}$$

where a and b are constant coefficients.

Under the above-mentioned assumptions, the MAF of the specified LS can be evaluated by the expression in Eq (4):

$$\lambda^j_{i,k} = \sqrt{\phi^j_{i,k}} k_{0,\ i,k}^{\ 1-\phi^j_{i,k}} \left[H_{i,k}\left(im^{\hat{C}^j}\right)\right]^{\phi^j_{i,k}} \cdot exp\left[\frac{1}{2} q_{i,k} k^2_{1,\ i,k}\left(\beta_C^{j\ 2} + \phi^j_{i,k}\beta^2_{D,\ i,k}\right)\right] \tag{3}$$

where, in addition to the symbols introduced above, the following parameters and symbols are used:

$$q_{i,k} = \frac{1}{1 + 2k_{2,\ i,k}\beta^2_{D,i,k} \Big/ b_{i,k}^{\ 2}} \tag{4}$$

$$\phi^j_{i,k} = \frac{1}{1 + 2k_{2,\ i,k}\left(\beta^2_{D,i,k} + \beta_C^{j\ 2}\right) \Big/ b_{i,k}^{\ 2}} \tag{5}$$

where $im^{\hat{C}}$ is the IM value for which $\widehat{D}=\widehat{C}$, and can be obtained from Eq (2) above as $im^{\hat{C}} = \left(\widehat{C}/a_{i,k}\right)^{1/b_{i,k}}$. The subscript i represents the Demand regime, the apex j represents the Capacity regime; the first concerns the main spatial direction of the action (e.g., horizontal/vertical for earthquake or different incident directions for wind), while the second is related to the Capacity level depending on the considered Limit State.

The index k represents the hazard (earthquake E or wind W). It is worth noting that in Eqs. (3-5) the conditioning of β_D from im has been eliminated by assuming a fixed and reasonable β_D value, for example one may choose to use a constant dispersion at the level of $IM = im^C$ (i.e., $\beta_D = \beta_{D|im} = \beta_{D|im^C}$).

Table 1 shows the basic steps to follow for the application of the SAC-FEMA method, which is the same regardless of the considered hazard (in the specific case of earthquake and wind). From the table it is possible to note the main differences in terms of considered Engineering Demand Parameter (EDP), IM, and hazard curve characterization. The Poisson and Weibull distributions are assumed to describe the hazard functions for earthquake and wind respectively, as commonly found in literature [19,21]. For specifics and further information on the SAC-FEMA probabilistic analysis method, the reader is addressed to the literature ([19, 21,22,23,24,25,26]); please note that there is no uniqueness of the choices made in relation to the monitoring parameter of the structural response (for example, this approach is well suited to the use of other EDPs for the assessment of structural performances).

For wind, as known and highlighted in the literature ([21,27,28, 29]), the angle θ of incidence assumes crucial importance, and in the case of prismatic buildings with a square section, two distinct aerodynamic regimes can occur, whose effects are to be considered predominant within certain sectors of the wind rose (Fig. 1a): these are the vortex shedding (VS) and buffeting (BU) aerodynamic regimes, and their sectors (α_{VS} and α_{BU}) are highlighted with blue and red contour respectively, while their hazard curves are qualitatively shown in Fig. 1b. Moreover, Fig. 1c represents one of the previously described steps of the SAC-FEMA method, which allows to obtain an algebraic and non-integral solution in the evaluation of the MAF of a certain limit state (i.e., the interpolation of the hazard curve using a 2° order formulation). It is also important to note that VS and BU regimes are characterised by different configurations of the wakes produced by the building (Fig. 2).

Specifically, the formulations shown in the table are declined for the two hazards as follows: for earthquake, if the vertical shaking is neglected, there will be only one hazard curve and MAF will thus be evaluated as Eq. (6)

$$\lambda_{i,E}^{SLS;ULS} = \sqrt{\phi_{i,E}^{SLS;ULS}} k_{0,i,E}{}^{1-\phi_{i,E}^{SLS;ULS}} \left[H_{i,E}\left(im^{\hat{C}^{SLS;ULS}}\right)\right]^{\phi_{i,E}^{SLS;ULS}} \cdot exp\left[\frac{1}{2} q_{i,E} k_{1,i,E}^2 \left(\beta_C^{SLS;ULS\,2} + \phi_{i,E}^{SLS;ULS} \beta_{D,i,E}^2\right)\right] \tag{6}$$

$i = horizontal$

For wind, typically the VS regime is critical for the comfort SLS due to the large floor accelerations induced in across-wind direction ([19, 28]). It follows that the interpolating forms of the hazard curves can be written as

$$H_{i,W}(im) = k_{0,\,i,W} exp\left(-k_{2,i,W} ln^2(im) - k_{1,i,W} ln(im)\right) \tag{7}$$

where: $k_{0,i,W}$, $k_{1,i,W}$ and $k_{2,i,W}$ are constant interpolation coefficients; the Demand can be assumed as

$$D_W = \mathrm{LN}(\widehat{D}_{i,W}, \beta_{D,i,W}) \tag{8}$$

being $\widehat{D} = a_{i,W} \cdot (im)^{b_{i,W}}$ and finally the MAF will be expressed as

$$\lambda_{i,W}^{SLS_{APT};SLS_{OFF}} = \mathrm{MAF} = \sqrt{\phi_{i,W}^{SLS_{APT};SLS_{OFF}}} k_{0,i,W}{}^{1-\phi_{i,W}^{SLS_{APT};SLS_{OFF}}} \left[H_{i,W}\left(im^{\hat{C}^{SLS_{APT};SLS_{OFF}}}\right)\right]^{\phi_{i,W}^{SLS_{APT};SLS_{OFF}}} \cdot exp\left[\frac{1}{2} q_{i,W} k_{1,i,W}^2 \left(\beta_C^{SLS_{APT};SLS_{OFF}\,2} + \phi_{i,W}^{SLS_{APT};SLS_{OFF}} \beta_{D,i,W}^2\right)\right] \tag{9}$$

Table 1
Assumptions concerning the SAC-FEMA analysis method for earthquake and wind.

SAC/FEMA Method	Earthquake	Wind
Limit States [LS]	SLS, ULS	SLS (occupants' comfort)
Intensity Measure[*IM*]	$S_a(T_1)$	V_{10}
Engineering Demand Parameter[*EDP*]	Interstory Drift Ratio [*IDR*]	Peak Acceleration [*PA*]
Hazard Distribution Function[*H-DF*]	Poisson	Weibull
Hazard Interpolation[*H-I*]	$H(s) = k_0\, exp[-k_2 ln^2(s) - k_1 ln(s)]$	
Demand[*D*]	Lognormal Distribution (η_D; β_D)	
Capacity[*C*]	Lognormal Distribution (η_C; β_C)	
Mean Annual Frequency [*MAF*]	$\lambda_{i,k}^j = \sqrt{\phi_{i,k}^j} k_{0,i,k}{}^{1-\phi_{i,k}^j} \left[H_{i,k}\left(im^{\hat{C}^j}\right)\right]^{\phi_{i,k}^j} \cdot exp\left[\frac{1}{2} q_{i,k} k_{1,i,k}^2 \left(\beta_C^{j\,2} + \phi_{i,k}^j \beta_{D,\,i,k}^2\right)\right]$	

Where:
i represents the Demand regime (related to the main spatial direction of the action);
j represents the Capacity regime due to the considered Limit State;
k represents the hazard (earthquake E, wind W);
SLS stands for Serviceability Limit State;
ULS stands for Ultimate Limit State;
$S_a(T_1)$ represens the spectral acceleration at the fundamental period of a structure;
V_{10} represents the mean wind velocity at 10 m above ground.

With i = incident wind direction and $j = SLS_{APT}$ or SLS_{OFF} indicates the considered SLS, for wich the capacity response threshold depends on the use of the building (APT = apartments, OFF = offices). Regarding the capacity, the distinction in different values is not due to the considered aerodynamic regime but to the intended use of the structure: in the literature the differentiation between apartments and offices is reported for the threshold values of frequency-dependent capacity, i.e. floor acceleration limit [30,31,32,33]. The definitive value to be used for the evaluation of the MAF, given the intended use j, is obtained by means of a weighted average of the MAFs identified for the two aerodynamic regimes evaluated (λ_{VS}^j; λ_{BU}^j), in which the weights are the occurrences (n_{VS} and n_{BU}) of the angle of incidence θ in the sectors of the wind rose in which the effects of vortex-shedding and buffeting are prevalent.

$$\lambda^j{}_W = \frac{\left(n_{VS}\ \lambda_{VS,W}^j + n_{BU}\ \lambda_{BU,W}^j\right)}{N_{TOT}},\ with\ N_{TOT} = n_{VS} + n_{BU} \tag{10}$$

As already said, for square buildings the main possible aerodynamic regimes are limited to VS and BU; moreover, wind incident sectors where either VS or BU dominate are easily identified by blue and red sectors respectively in Fig. 1a, including mixed regimes as explained in already mentioned previous publications [21]. Wind speed statistic and corresponding structural response belonging to different sectors can be separately collected in order to have separated MAFs evaluations (including hazard curves, demand and capacity parameters evaluation) to be finally weighted averaged as represented in eq. (10). In general, the occurring of different aerodynamic regimes depends mainly on the building geometry/aerodynamic shape given at a certain incident wind direction, and the identification of the related incidence sectors in the wind rose has to be made by appropriate wind tunnel tests or

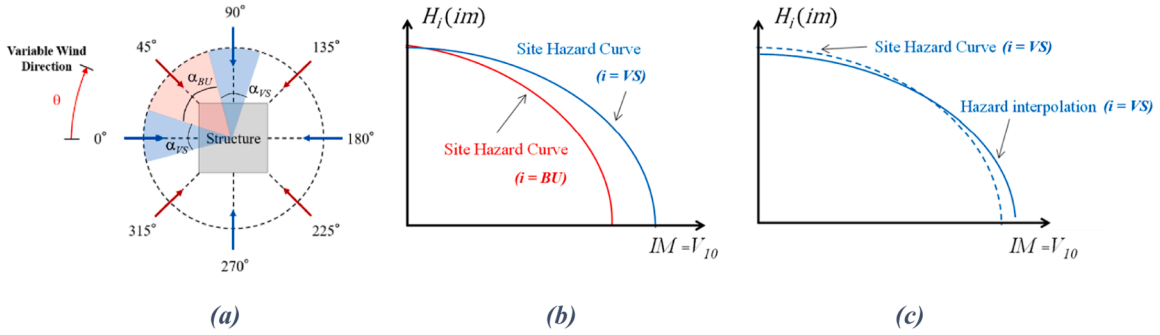

Fig. 1. (a) Wind angles of incidence related to different aerodynamic regimes [21]; (b) hazard curves associated to different aerodynamic regimes by the site climatology; (c) hazard interpolation.

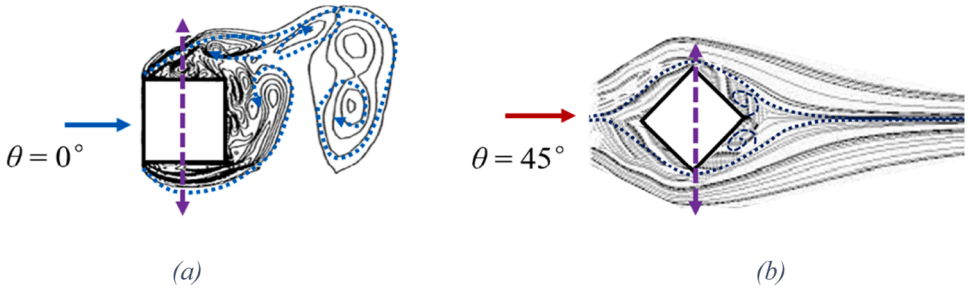

Fig. 2. (a) VS aerodynamic regime (adapted from [28]); (b) BU aerodynamic regime (adapted from [28]).

computational fluid dynamic analyses [27]. In addition, the use of the above-mentioned tunnel or computational fluid dynamic analyses can lead to assess responses which are governed by aerodynamic effects other than VS and BU. In these cases, the regimes can be treated as additional cases together with (or instead of) VS and BU.

Thus, with specific reference to wind and earthquake, the issue related to the unification of the performance evaluation framework for the various hazards, is addressed. Using the afore mentioned SAC-FEMA method for both earthquake and wind, the structural performances are evaluated by a unified procedure and expressed with the same metrics (MAF) for the occurrence of a certain limit state LS. Performances of steel frames with different heights (low and high-rise buildings) will be assessed in next sections in the view of the ULSs and SLSs and in order to determine the relative importance of different hazards in the structural response.

2.2. Wind analysis

Two different formulations have been considered for the purpose of evaluating the spectra of along-wind and across-wind turbulence, associated with the two different aerodynamic regimes: the first is the one proposed by Solari and Piccardo 2001 [34] and Carassale and Solari 2006 [35], also present in [36] and [37], while the second is the one proposed by Liang et al. (2002) [38], specific for identifying dynamic loads acrosswind in the case of tall buildings with a square or rectangular section. Considering the first formulation and by neglecting the vertical component w of the wind velocity, the turbulent components u and v can be identified in "N" spatial locations by the power spectral density matrices $\boldsymbol{S_l}$ ($l = u, v$) (where u and v represent the horizontal turbulent component of the wind velocity, respectively in X and Y direction). The diagonal terms (auto-spectra) $S_{l_q l_q}(n)$ of $\boldsymbol{S_l}$ are expressed in terms of the normalised one-side power spectral density as

$$\frac{nS_{u_q u_q}(z,n)}{\sigma_u^2(z)} = \frac{6.868\ n_u(z_q)}{\left[1+10.302\ n_u^2(z_q)\right]^{5/3}} \tag{11}$$

$$\frac{nS_{v_q v_q}(z,n)}{\sigma_v^2(z)} = \frac{9.434\ n_v(z_q)}{\left[1+14.151\ n_v^2(z_q)\right]^{5/3}} \tag{12}$$

Where: n is the frequency (Hz), z_q (m) is the height of the point q, σ_u^2 and σ_v^2 are the variances of the velocity fluctuations (Solari and Piccardo 2001) [34]

$$\sigma_u^2 = [6 - 1.1\ arctan(ln(z_0) + 1.75)]\ u_*^2 \tag{13}$$

$$\frac{\sigma_v}{\sigma_u} = 0.75 \tag{14}$$

u_*^2 is the friction or shear velocity (in m/s), given by: $[(K)^{1/2}\ V_{10}]$, where K is a coefficient depending on the roughness length z_0, V_{10} is the 10-mins average wind velocity at 10 m height and $n_l(z_q)$ is a non-dimensional height dependent frequency given by:

$$n_l(z_q) = \frac{nL_l(z_q)}{V_m(z_q)} \tag{15}$$

and the integral scales $L_l\ (z_q)$ of the turbulent components have been derived for $l = u, v$ according to the procedure given in [39]. The terms outside the diagonal (cross-spectra) $S_{l_q l_r}(n)$ of $\boldsymbol{S_l}$ are instead identified as

$$S_{l_q l_r}(n) = \sqrt{S_{l_q l_q}(n) S_{l_r l_r}(n)}\ exp\Big(-f_{qr}(n)\Big) \tag{16}$$

With

$$f_{qr}(n) = \frac{|n|\ C_z|z_q - z_r|}{V_m(z_q) + V_m(z_r)} \tag{17}$$

Where C_z is a coefficient inversely proportional to the spatial correlation of the process (decay coefficient). The force spectra matrix $\boldsymbol{S_{FF}}$ is obtained multiplying the terms of the velocity spectra matrix $\boldsymbol{S_l}$ by $\left(\rho_{air}^2 \cdot c_{drag}^2 \cdot A_{infl}^2 \cdot v_m^2\right)$, where ρ_{air} is the air density (assumed equal to 1.25 kg/m^3), c_{drag} is the drag coefficient equal to 1.05 in what follows (which

depends on the section of the structure, here assumed squared), A_{infl} represents the tributary area of the node subjected to the wind load, and, finally $V_m(z_q)$ and $V_m(z_r)$ represent the mean velocities proportional to the height with respect to the ground, at height z_q and z_r for points q and r respectively.

Regarding the VS regime, according to the analytical formulation proposed by Liang et al. [38], the total across wind force spectra at a location j is given by

$$S_{F_v F_v}(n, z_q, z_q) = \frac{\sigma(z_q)^2}{n}\left[\frac{\overline{A}\, H(C_1)\overline{n}^2}{(1-\overline{n}^2)^2 + C_1\overline{n}^2} + \frac{(1-\overline{A})\sqrt{C_2}\overline{n}^3}{1.56\left[(1-n^2)^2 + C_2\overline{n}^2\right]}\right], \quad (q = 1,\ K,\ N_f) \tag{18}$$

The first term represents the effect of turbulence and the second term the effect of vortex shedding. In the previous equation (Eq. (18)), $\sigma(z_q)$ is the root mean square of the across wind force at floor q, expressed as

$$\sigma(z_q) = \frac{1}{2}\rho\ V_m^2(z_q)\ \overline{C}_L\ B\ \Delta z_q \tag{19}$$

where Δz_q indicates the tributary height for the floor q, i.e., half upper interstorey plus half lower interstorey, B is the width of the building, $\overline{C}_L$ is mean of the lift coefficient, $\overline{A}$ is the power-assignation coefficient

$$\overline{A} = \frac{H}{\sqrt{S}}\left[-0.118\left(\frac{D}{B}\right)^2 + 0.358\left(\frac{D}{B}\right) - 0.214\right] + \left[0.066\left(\frac{D}{B}\right)^2 - 0.26\left(\frac{D}{B}\right) + 0.894\right] \tag{20}$$

D is the length of the building, S is the cross-sectional area, H is the total height of the building, $\overline{n} = \frac{n}{n_s}$ and $n_s = \frac{S_t V_m(z_q)}{B}$ is the frequency of vortex shedding determined by the Strouhal number S_t;

$$\mathrm{H}(C_1) = 0.179\ C_1 + 0.65\sqrt{C_1} \tag{21}$$

where C_1 is a parameter correlated to bandwidth expressed as

$$C_1 = \frac{\left[0.47(D/B)^{2.8} - 0.52(D/B)^{1.4} + 0.24\right]}{(H/\sqrt{S})} \tag{22}$$

And C_2 is equal to 2. Finally, the coherence between the across wind forces at locations m and n can be approximated as

$$r_{mn} \cong exp\left[-\left(\frac{\Delta}{\delta}\right)^2\right] \tag{23}$$

Where $\Delta = |z_q - z_r|/B$ and δ is a constant that depends on ratio D/B.

The response PSD matrices of displacement (x) and acceleration $(\ddot{x})$ defined by the ***M, C***, and ***K*** matrices due to the force spectra formulations assumed are obtained, under the assumption of linear structural behavior, using the frequency domain input-output relationships of random vibrations (e.g., Soong and Grigoriu 1993 [40])

$$\boldsymbol{S}_{xx}(2\pi/n) = \boldsymbol{B}(2\pi/n)^* \boldsymbol{S}_{FF}(2\pi/n)\boldsymbol{B}(2\pi/n) \quad \text{and} \quad \boldsymbol{S}_{\ddot{x}\ddot{x}}(2\pi/n) = \omega^4 \boldsymbol{S}_{xx}(2\pi/n), \tag{24}$$

In Eq. (24), $\boldsymbol{S_{FF}}$ is the PSD wind force matrix obtained by the previously introduced relationships. Further, the "*" superscript denotes complex matrix conjugation, and the transfer matrix B is given as

$$\boldsymbol{B}(2\pi/n) = \left[\boldsymbol{K} - (2\pi/n)^2\boldsymbol{M} + i(2\pi/n)\boldsymbol{C}\right]^{-1} \tag{25}$$

where, $i = \sqrt{-1}$ and K and M are the stiffness and mass matrices of the building respectively. The response displacement and acceleration variances of the r-th floor for the structure are obtained, respectively, as

$$\sigma_{x_r}^2 = \int_0^{(2\pi/n)_{max}} S_{x_r x_r}(2\pi/n)d(2\pi/n) \text{ and } \sigma_{\dot{x}_r}^2 = \int_0^{(2\pi/n)_{max}} S_{\ddot{x}_r\ddot{x}_r}(2\pi/n)d(2\pi/n) \tag{26}$$

The response auto-spectra populating the main diagonal elements of the response PSDs in Eq. (24) on the frequency axis is integrated up to a maximum (cut-off) frequency $\omega_{max} = (2\pi/n)_{\max}$ above which the energy of the underlying processes becomes negligible. The variance of the relative acceleration response between two different floors (or DOFs) q and r, $\ddot{x}_q - \ddot{x}_r$, is obtained as [40]

$$\sigma_{\ddot{x}_{qr}}^2 = \sigma_{\ddot{x}_q}^2 + \sigma_{\ddot{x}_r}^2 - 2\int_0^{(2\pi/n)_{max}} S_{\ddot{x}_q\ddot{x}_r}(2\pi/n)d(2\pi/n) \tag{27}$$

where the integrand is the acceleration response cross-spectrum corresponding to the q and r DOFs. Finally, peak q-th floor displacements and accelerations and peak relative acceleration between q and r floors, are estimated by the expressions

$$\max\{x_q\} = g\sqrt{\sigma_{x_q}^2}, \quad \max\left\{\ddot{x}_q\right\} = g\sqrt{\sigma_{\ddot{x}_q}^2}, \quad \text{and} \quad \max\left\{\ddot{x}_{qr}\right\} = g\sqrt{\sigma_{\ddot{x}_{qr}}^2} \tag{28}$$

respectively. In the above expressions, g is the peak factor estimated by the widely used empirical formula due to Davenport (1964) [41,42]

$$g = \sqrt{2ln(\eta T_{wind})} + \frac{0.577}{\sqrt{2ln(\eta T_{wind})}} \tag{29}$$

where $\eta = \omega/2\pi$ is the effective structural response frequency in Hz (e.g., can be taken equal to the fundamental natural frequency of the primary structure), and T_{wind} is an assumed time duration of exposure to the wind action during which the peak response quantities in Eq. (29) are evaluated (3600 s). The latter consideration implies that the underlying stochastic input/output processes are quasi-stationary (i.e., stationary/ergodic time-limited processes).

2.3. Seismic analysis

The use of non-linear time-history analysis (NLTHA) for assessing structural performances under earthquake implies a high computational

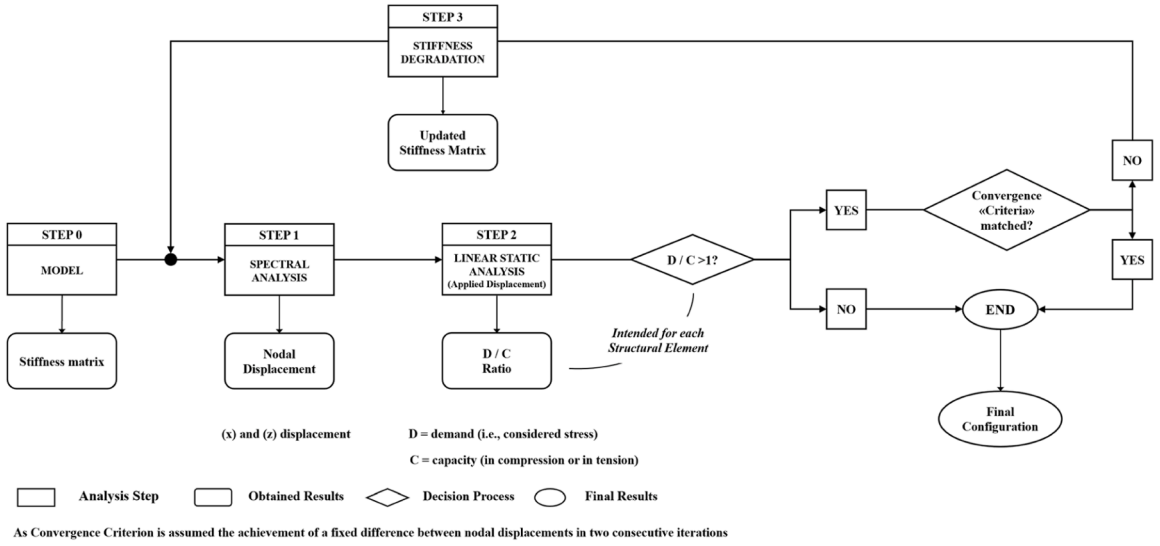

Fig. 3. Iterative procedure for the element-by-element degradation of the stiffness matrix depending on the excursion in the plastic range and on the local buckling.

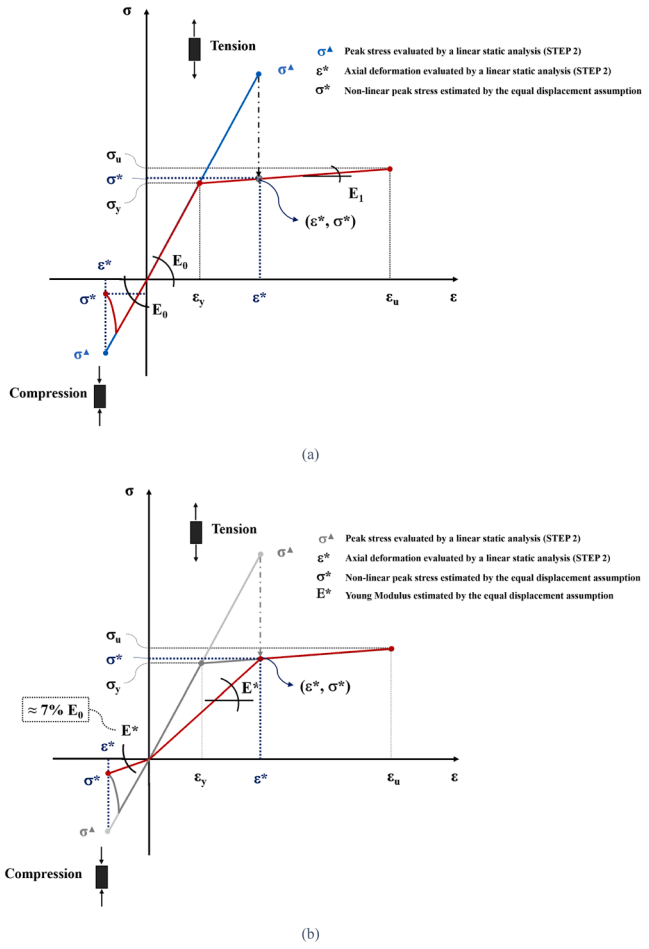

Fig. 4. Stiffness degradation procedure for slender elements: (a) equal displacement assumption; (b) evaluation of the reduced elastic modulus.

burden. To avoid this drawback an iterative response spectrum linear dynamic analysis enhanced by an element-by-element stiffness degradation procedure has been implemented to take into account plastic non-linear behaviours. The element-by-element stiffness degradation depends on the demand excursion in the plastic range and to the local buckling occurrence (both identified by the Demand versus Capacity ratio, D / C). The procedure, which consists of several steps and is shown in the exemplary flowchart (Fig. 3), has been already introduced in literature for reinforced concrete buildings ([25,43]) and it has therefore been adapted here for plane steel frames with shear resisting connections, where excursion in the plastic range and buckling phenomena are expected to occur in bracing elements or in columns.

In step 1 a linear spectral response analysis is carried out. The absolute values of nodal displacements are then identified and stored. The capacity considered for columns, bracing elements and outriggers must be differentiated in the two cases of tension and compression due to the possible buckling of the compressed elements.

To evaluate stresses, the displacements obtained in step 1 are applied to the structure by carrying out a linear static analysis (step 2); in this way it is possible to compare the tensile and compressive stresses in each structural element (which represents the actual "D") with their capacity "C", equal to the buckling strength (S_B) in the case of compressed, slender elements, and the yielding strength (S_y) in the case of non-slender elements. In step 3 the deformation state of each element (axial deformation ε) is monitored: to implement the stiffness degradation in cases where the D / C ratio exceed one, the following assumptions are made (see Fig. 4):

- if the element is slender ($|S_B| < |S_y|$) and it is compressed ($\varepsilon < 0$), the value of the element elastic modulus E is reduced to the 7 % of its original value, which is calibrated to consider the significant stiffness reduction of slender elements when buckled and, at the same time, to avoid analysis convergence problems arising at lower values;
- if the element is slender ($|S_B| < |S_y|$) and it is in tension ($\varepsilon > 0$), or if the element is not slender ($|S_B| > |S_y|$) either the element is in compression ($\varepsilon < 0$) or in tension ($\varepsilon > 0$), the so-called equal displacement assumption is implemented to evaluate the secant elastic modulus E* to be assigned to the element given the elastic stress $\sigma^{\blacktriangle}$ evaluated by the linear static analysis carried out at step 2.

The step 3 is iterated until convergence (the difference between the displacements of the previous and current iterations is lower than the fixed threshold).

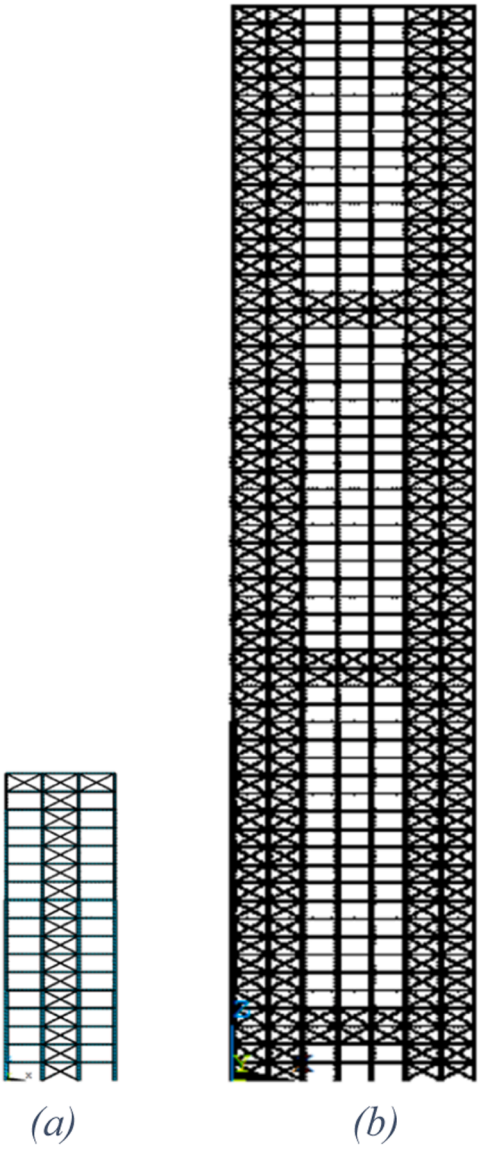

Fig. 5. 2D steel buildings of different heights considered in the application: (a) 17 floors; (b) 60 floors.

3. Application

3.1. Description of case studies

The implementation of the proposed SAC-FEMA method for the performance evaluation of steel buildings allows to use a unique framework for different hazards. From a M-H perspective, then, it makes sense to exploit the method to evaluate how conflicting design solutions required by the two hazards drive the design and how dominant hazard varies considering different buildings height. These assessments were made on two 2D steel shear-resisting frames (Fig. 5) of different heights (17 floors – 59.5 m and 60 floors – 210 m) to evaluate how the increased flexibility of the building has an influence on the design choices and on the dominant hazard between the considered ones. The studied frames are to be intended as belonging to 3D structures (of which they are the most-braced elements) and are assumed to be representative of the global structural response ([44,45,46]).

These are shear-resisting frames, for which the initial configuration is identified following a pre-sizing for vertical loads only, considering a precautionary use of C/D utilization coefficients for the structural elements (for U.L.S. combination: bracing system and outriggers 30 %, columns 60 %, beams 30 %). Table 2 shows the elements' cross sections used in the aforementioned initial configurations for the considered plane frames. Note that out-of-plane deformations are disabled and that beam-column joints and beam-column-outrigger trusses (or bracing system trusses) are modelled as "hinges".

Table 2
Initial configuration of the different plane frames considered.

Initial Configurations				
N Floors	17		60	
H Interstory [m]	3.5		3.5	
L Bays [m]	6		6	
H TOT [m]	59.5		210	
BEAMS	IPE 360		IPE 360	
COLUMNS	Floors	Section	Floors	Section
	1 - 5	HEB 700	1 - 30	double HEM 900
	6 – 10	HEB 600	31 - 60	double HEB 650
	11 - 15	HEB 500		
	16 - 17	HEB 400		
N° OF BRACING SYSTEM	1		4	
BRACING SYSTEM	Floors	Section	Floors	Section
	1 - 5	Steel tube 273 × 20	1 - 30	Steel tube 508 × 10
	6 – 10	Steel tube 244 × 20	31 - 60	Steel tube 406.4 × 10
	11 - 15	Steel tube 219.1 × 20		
	16 - 17	Steel tube 219.1 × 16		
N° OF OUTRIGGERS	1		6	
AT FLOOR:	17		3 – 4 – 23 – 24 – 43 – 44	

Table 3
Interpolation coefficients used for hazard curves.

	Seismic Hazard	Wind Hazard	
		Buffeting	Vortex Shedding
k_0	0.013	4.6e-18	9e-14
k_1	1.96	−36.13	−26.55
k_2	0.234	7.96	6.07

3.2. Hazard analysis

For demonstration purposes, the case study buildings are located in a site with high seismicity and high wind; in particular, it is considered an ideal site whose seismic hazard is from L'Aquila (Italy) and the wind hazard is from Orlando, Florida (U.S.A.) (the details regarding the wind-hazard characterization, i.e., Weibull parameters for the wind velocity along different sectors of the wind rose, are provided in Petrini & Ciampoli (2012) [47]). The parameters used in the second order equations for the interpolation of hazard curves by using Eq. (1) are reported in Table 3, determining the curves presented in Fig. 6a) and b).

3.3. Performance indicators and limit state identifications

Fig. 7 and Table 4 show a summary of the analysis process carried out for both considered hazards, starting from the parameter used to define the intensity of the hazard (V_{10} for wind, $Sa(T_1)$ for earthquake), the type of analysis performed (PSD Analysis for wind and Spectrum analysis for earthquake), the monitored EDP (Interstory Drift Ratio for earthquake and Across-wind peak acceleration for wind), the considered limit states (SLS and ULS for seismic analysis and comfort SLS for wind analysis) as identified by appropriate response thresholds for the EDPs, and the limit values for their MAFs.

k_2	0.234	7.96	6.07

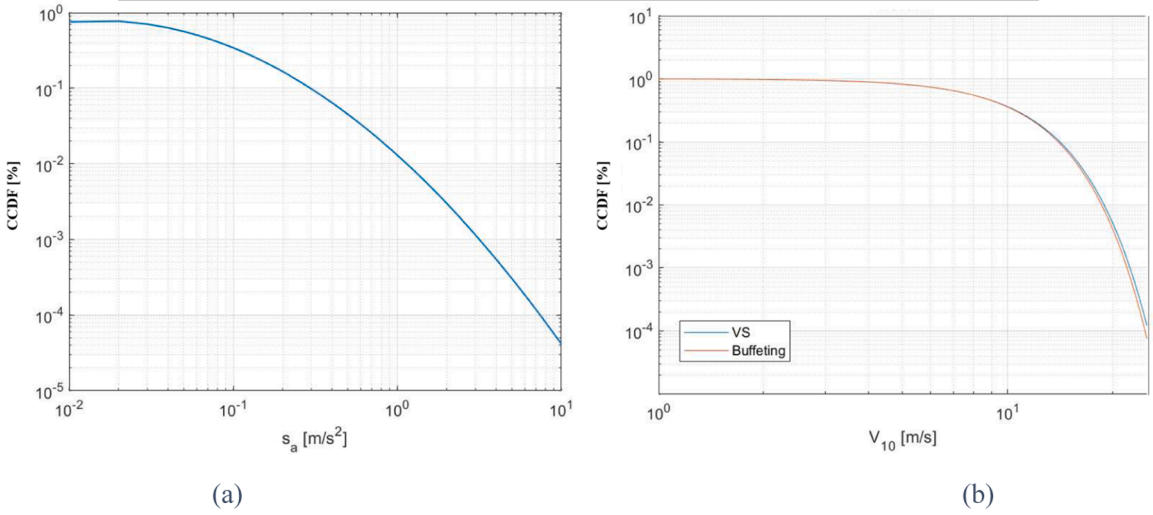

Fig. 6. Earthquake (a) and wind (b) hazard curves.

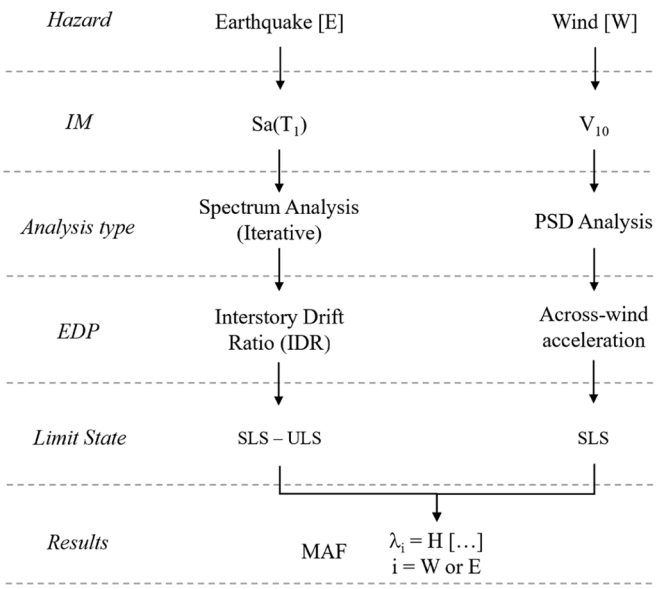

Fig. 7. Summary of the analysis paths carried out for the two hazards considered.

Table 4
EDP limit values and MAFs limit values considered.

Earthquake		Wind
EDP (IDR) Limit		EDP (Acrosswind peak acceleration) Limit
SLS	ULS	SLS
$\delta^E_{SLS} = 0.0033$	$\delta^E_{ULS} = 0.02$	Frequency dependent
MAF_{Limit}		MAF_{Limit}
$\lambda^E_{SLS} = 0.02$	$\lambda^E_{ULS} = 0.001$	$\lambda^W_{SLS} = 0.01$
$\lambda^E_{SLS} = 0.01$	$\lambda^E_{ULS} = 0.0004$	

The acceptability of the performance is assessed by comparing the obtained MAF values with the appropriate threshold values. It should therefore be noted that the two analysis procedures converge in a single comparable performance evaluation metric which is the MAF obtained using a SAC-FEMA approach.

For the analyses under earthquake two limit states are considered, one of which is associated with a low level of damage (SLS) and one associated with a high level of damage (Collapse Prevention – ULS); with regard to the median capacity values of the considered EDP (the inter-floor drift), it is assumed from the literature ([25,32,48]) $\delta^E_{SLS} = 0.0033$ e $\delta^E_{ULS} = 0.02$. The values of the corresponding MAFs were assumed arbitrarily equal to $\lambda^E_{SLS} = 0.02$ e $\lambda^E_{ULS} = 0.001$ for the 17-Floors frame, while $\lambda^E_{SLS} = 0.01$ e $\lambda^E_{ULS} = 0.0004$ are assumed for the 60-store frame.

As regards the wind analyses, on the other hand, only one limit state is considered, the one related to the comfort of the occupants; the capacity threshold value (across-wind induced peak acceleration) are obtained from the graphs that report occupant comfort limit state [49,50]. These threshold values depend on the structure's fundamental frequency ($\widehat{C}^{APT}_{17\ FLoors} = 0.06$ m/s^2, $\widehat{C}^{OFF}_{17\ FLoors} = 0.088$ m/s^2; $\widehat{C}^{APT}_{60\ FLoors} = 0.09$ m/s^2 $\widehat{C}^{OFF}_{60\ FLoors} = 0.14$ m/s^2. Thus, it is assumed $\lambda^W_{SLS} = 0.01$.

3.4. Uncertainties modeling

The quantification and modeling of uncertainties is a fundamental step in the application of the SAC-FEMA method; for the purposes of this application, given the classic distinction between aleatory uncertainties and epistemic uncertainties, the latter are assumed equal to zero.

Regarding the earthquake, the capacity dispersion β_C is assumed

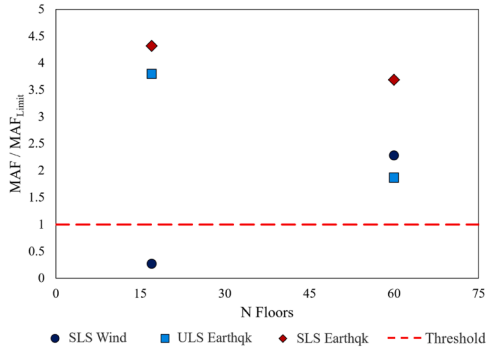

Fig. 8. Evaluation of MAF/MAFLimit for the initial configurations of the different steel plane frames considered.

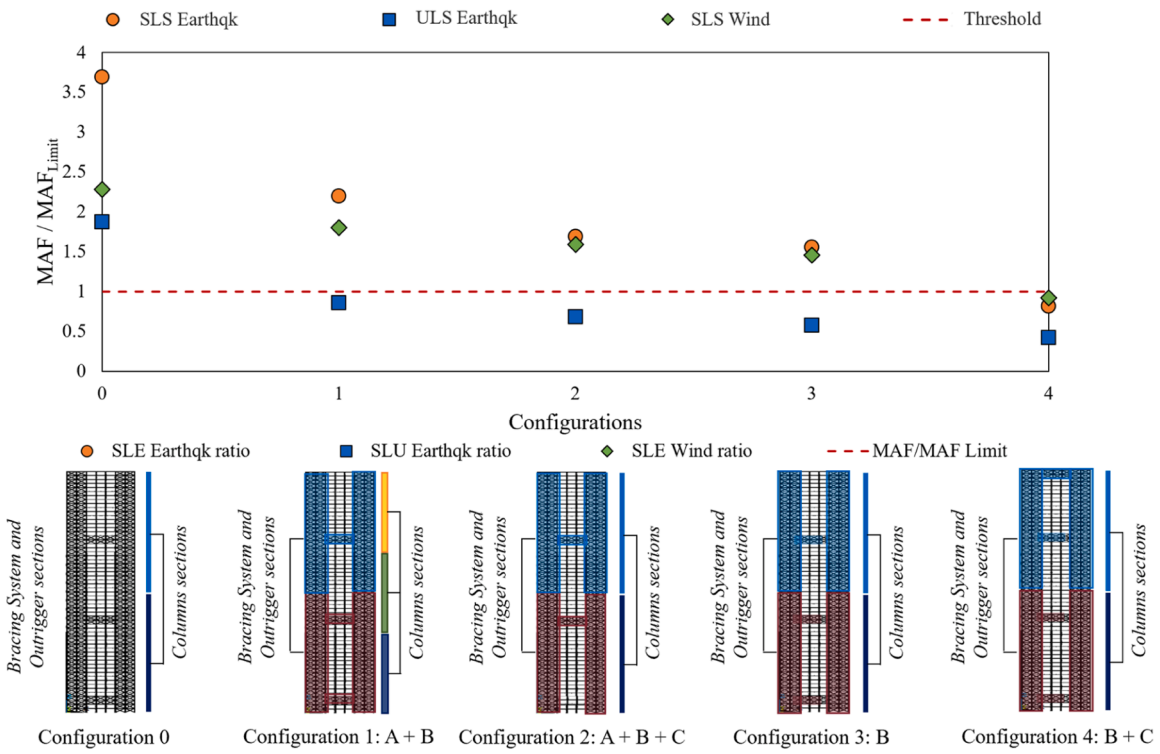

Fig. 9. Evaluation of MAF/MAF$_{Limit}$ for different design configurations of the 60-Floors steel plane frame.

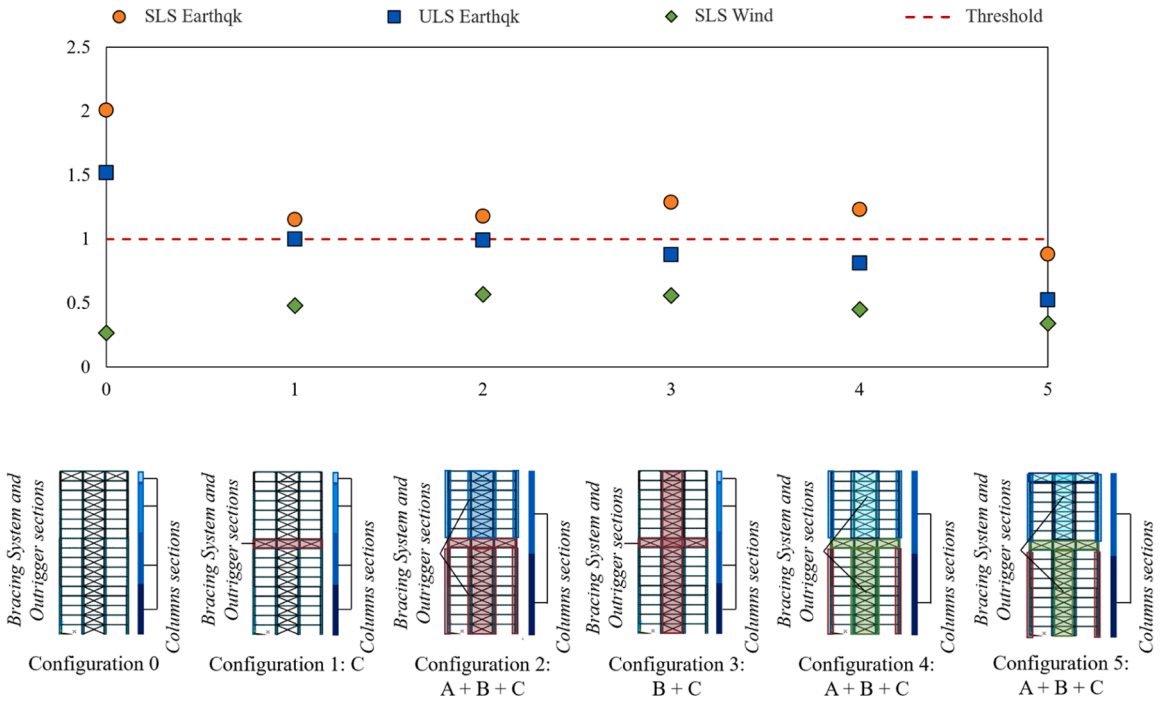

Fig. 10. Evaluation of MAF/MAF$_{Limit}$ for different design configurations of the 17-Floors steel plane frame.

[22] equal to $\beta_C = 0.35$ for extensive damage level (ULS limit state) and equal to $\beta_C = 0$ for slight damage level (SLS limit state). On the other hand, with regard to the demand dispersion β_D, it can be assumed from literature [21] as $\beta_D = 0.4$ for the 17-floors frame and to $\beta_D = 0.37$ for the 60-floors frame.

Regarding the wind, the capacity depends on many different factors [51], as the frequency of the structure and the percentage N_p of the floor occupants that perceives the building motion. The capacity threshold value for the considered EDP (acrosswind peak acceleration) is strictly related to the main structural frequency; entering the graphs of the perception threshold curves (from literature) with the fundamental frequency of the considered structure, it is possible to obtain a samples statistical distribution of the aforementioned perception thresholds and then approximate it to a lognormal distribution [21] in order to

determine its characteristic parameters (median value and dispersion). Thus, it is obtained $\beta_C^{APT} = 0.48$; $\beta_C^{OFF} = 0.31$ [15]. The demand dispersions are assumed from literature [21] equal to $\beta_{D-VS} = 0.45$ and $\beta_{D-BU} = 0.25$.

3.5. MAF evaluation for initial configurations

Using the same performance evaluation metrics/performance indicators, it is possible to report the results in a single graph, monitoring the structural behaviour under different hazards simultaneously. Once the considered LSs and the threshold values (both for EDPs and MAFs) have been defined, the performances of the different structures can be appropriately defined as the MAF / MAF_{Limit} ratio: in this way, values greater than one represent unacceptable performances, while values lower than one represent acceptable performances (Fig. 8). The analysis of the initial configurations shows that as the height of the buildings increases, the sensitivity to the considered hazards changes: the 17-storey frame provides acceptable performances (already in the initial configuration) towards the wind and unacceptable performances against the earthquake, while the 60-storey frame presents comparable unacceptable performance for both hazards and for all the considered LSs.

3.6. Multi-hazard design

The definition of appropriate design solutions by simultaneously taking into account the performance of building structures under the two hazards can be carried out on the basis of what shown in Figs. 9-10, where performance indicators for different design iterations carried out for the 60 and 17 storey frames respectively are highlighted. Design modifications made to the initial configurations (configuration n°0 in figures, whose details are reported in Table 2) can be divided into the following categories: (A) variation of the sections of the columns, (B) variation of the sections of the bracing elements and of the outriggers, (C) variation of the location, removal or addition of outrigger. For the 60-storey frame (Fig. 9), 5 different design solutions were considered in order to identify an "optimal" configuration for which a MAF / MAF_{Limit} ratio close to the unit value for the considered LSs. Specifically, configuration 1 foresees, compared to the initial configuration (n°0), a strengthening of the sections of the bracing elements (floors 1–30 steel tube 610 × 32 mm^2 section; floor 31 – 60 steel tube 559 × 32 mm^2 section); also, the columns' sections are slightly different: there is no longer a tapering every 30 floors, but every 20. From the first to the 20th floor, double HEB 900 are used (as in configuration n°0 from floor 1 to 30), from the 21st to the 40th floor a double HEB 650 section is used (as in configuration n°0 from floor 31 to 60) and the last 20 floors are characterised by a double HEB400. Configuration 2 compared to the n°0 provides for the removal of the first level of outriggers and at the same time a strengthening of the bracing system sections (floors 0 – 30: double HEB900 as column sections and 610 × 32 mm^2 steel tube as truss sections; floors 31 – 60: double HEB650 as column sections and 559 × 32 mm^2 steel tube as truss sections); finally configurations 3 and 4 have the same sections used for 2 but the number of outriggers varies (3 levels in configuration 3, and 4 levels in configuration 4). The outrigger trusses sections are the same of the ones used for the bracing system elements at same height; the section used for the beams is always the same (see Table 2) and kept for every floor. As can be seen from Fig. 9, in the case of configuration 4 the MAF / MAF_{Limit} ratios are close to one: the implementation of an additional outrigger in the last floor of the structure is much more effective for both hazards than the variation of the sections of the bracing blades and columns.

For the 17-storey frame (Fig. 10), 5 design solutions were considered: compared to the initial configuration (n° 0), configuration 1 provides for a simple relocation of the outrigger from the seventeenth to the tenth floor; configurations 2, 3 and 4 provide for a progressive strengthening of the structure due to the variation of the inertial properties of the cross-sections, keeping the position of the outrigger unchanged (10th floor); in particular, in the configuration 2 for the first 10 floors are used a steel tube section 237 × 20 mm^2 (trusses of the bracing system and of the outrigger) and an HEB700 steel section (columns), while for the remaining floors, a 244 × 20 mm^2 steel tube section and an HEB600 steel section are considered. In the configuration n° 3 the columns have the same section of the configuration n°0, while just one steel tube section is used for both bracing system and outrigger trusses (329.4 × 20 mm^2). In the configuration 4, two sections are considered for columns (HEB700 and HEB600) and two tube sections are used for the bracing system and outrigger trusses (323.9 × 25 mm^2 and 273 × 25 mm^2); in both cases, the change of the sections occurs between the 10th and the 11th floors. Finally, configuration 5 is obtained from the configuration 4 by adding an additional outrigger (characterised by a tube section 273 × 25 mm^2) on the top floor. As in the previous case, the section used for the beams is always the same (see Table 2) and kept for every floor. In this case it can be noted that this structure is essentially insensitive to the wind even when the structural configurations vary, since the MAF / MAF_{Limit} ratio can be considered constant (and always less than one); as regards the earthquake, on the other hand, the sensitivity to the hazard is noticeable: changes in the configuration lead to a progressive stiffening of the structure, determining a progressive variation of the obtained MAF value. If the mere variation of the sections of the structural elements is not effective in obtaining configurations close to the optimal one, the insertion of a global stiffening element (such as the outrigger) can be convenient.

The opposite/competitive design strategies concept can be understood considering the frequency-dependent energy content of the two actions' spectra [52]: as the height of the building increases, the relevance of the effects induced by the wind increases as well [53], while the earthquake's relevance decreases. The analysis of the 17storey building as second case study is inserted just to explain the concept by showing that this building is insensitive to one of the two hazards and then does not pose any competitive design strategy.

4. Conclusion

In this work a framework for the design case of medium-rise low-damped steel buildings under earthquake and winds is proposed, then addressing one of the key issues of MH design (i.e., unified framework problem): a unique metric for the assessment of structural performances under wind and earthquake loads is considered. This case represents the typical interaction between independent hazards, which can determine the occurrence of some opposite/competitive design strategies. It is indeed interesting to have a reliable approach which can produce a truly PB-MH Design, determining the best design configuration by considering both SLSs and ULSs for all the acting hazards, especially for relevant structures whose unsatisfactory performances can lead to significant social and economic impacts. The proposed method is based on a SAC-FEMA approach, which allows to evaluate with simplified analytical calculation the Mean Annual Frequency (MAF) for a certain Limit State (LS) using Demand versus Capacity format. This method has in fact been originally developed for seismic-analyses and, recently, proposed for wind-analyses, and this case represents the first application of SAC-FEMA methods to a MH case, with structural performances under different hazards expressed using the same metrics. Considering two different 2D structures (60-story and 17-story), possible design choices made to reach comparable reliability levels against earthquake and wind, which guarantee MAFs close to acceptable occurrences for all LSs, are assessed. Thus, from the analysis of frames it is possible to understand the potential of a MH design, especially when the considered hazards are both relevant in driving design choices (i.e., 60-story examined buildings), since an equal design strategy might have different consequences depending on the properties of the considered structures. This procedure also allows to obtain a Standards-oriented probabilistic PBE formats that are applicable to a broad band of LSs and structural typologies and at the same time affordable for real-world

design application.

CRediT authorship contribution statement

M. Francioli: Writing – original draft, Formal analysis. **F. Petrini:** Writing – review & editing, Supervision, Methodology, Funding acquisition, Conceptualization.

Declaration of competing interest

The authors declare that they have no known competing financial interests or personal relationships that could have appeared to influence the work reported in this paper.

Acknowledgement

The authors acknowledge the financial support of the Research Project "Multi-hazard Optimal DEsign and Reliability Analysis of sTEel buildings (MODERATE)" [Bandi di Ateneo 2021- ID: RM12117A5BC54913] and PNRR (Piano Nazionale di Ripresa e Resilienza) funding scheme as part of the National Research Centre CN1 on "High-Performance Computing, Big Data and Quantum Computing" - Spoke 5 – "Environment and Natural Disaster: Framework and methodologies for impact evaluation and risk mitigation" [Research Project No. CN1221844D08208F from Sapienza University of Rome, Directorial Decretation no. 1031 of June, 17th, 2022].

References

[1] Guo X, Zhang H, Li H, Yuan X, Ding Y. Multi-hazard performance assessment of low-rise cold-formed steel structures subjected to combined earthquake and wind. J Constr Steel Res 2024;214:108501. https://doi.org/10.1016/j.jcsr.2024.108501. 2024.
[2] UNISDR (United Nations International Strategy for Disaster Reduction) 2015. Sendai framework for disaster risk reduction 2015-2030. Geneva.
[3] UNI, EN. Eurocode 0 – basis of structural design. European Committee for Standardization; 2006.
[4] Cavalieri F, Franchin P, Giovinazzi S. Multi-hazard assessment of increased flooding hazard due to earthquake-induced damage to the natural drainage system. Reliability Engineering and System Safety 2023;237:109348. https://doi.org/10.1016/j.ress.2023.109348. 2023.
[5] He Z, Shen K, Lan M, Weng W. The effects of dynamic multi-hazard risk assessment on evacuation strategies in chemical accidents. Reliability Engineering and System Safety 2024;246:110044. https://doi.org/10.1016/j.ress.2024.110044. 2024.
[6] Fang C, Xu YL, Li Y, Li J. Serviceability analysis of sea-crossing bridges under correlated wind and wave loads. Reliability Engineering and System Safety 2024;246:110077. https://doi.org/10.1016/j.ress.2024.110077. 2024.
[7] Li X, Chen G, Amyotte P, Khan F, Alauddin M. Vulnerability assessment of storage tanks exposed to simultaneous fire and explosion hazards. Reliability Engineering and System Safety 2023;230:108960. https://doi.org/10.1016/j.ress.2022.108960. 2023.
[8] Krausmann E, Girgin S, Necci A. Natural hazard impacts on industry and critical infrastructure: Natech risk drivers and risk management performance indicators. Int J of Dis Risk Red 2019;40. https://doi.org/10.1016/j.ijdrr.2019.101163.
[9] Francioli M, Petrini F, Bontempi F. Structural robustness analysis of RC frames under seismic and blast chained loads scenarios. Journal of Building Engineering 2023;67. https://doi.org/10.1016/j.jobe.2023.105970.
[10] Celano F, Dolšek M. Fatality risk estimation for industrialized urban areas considering multi-hazard domino effects triggered by earthquakes. Reliability Engineering and System Safety 2021;206:107287. https://doi.org/10.1016/j.ress.2020.107287. 2021.
[11] Gupta HS, Adluri T, Sanderson D, González AD, Nicholson CD, Cox D. Multi-objective optimization of mitigation strategies for buildings subject to multiple hazards. International Journal of Disaster Risk Reduction 2024;100:104125. https://doi.org/10.1016/j.ijdrr.2023.104125. 2024.
[12] Hao H, Bi K, Chen W, Pham TM, Li J. Towards next generation design of sustainable, durable, multi-hazard resistant, resilient, and smart civil engineering structures. Eng Struct 2023;277:115477. https://doi.org/10.1016/j.engstruct.2022.115477. 2023.
[13] Men J, Chen G, Reniers G, Wu Y, Huang H. Experimental and numerical study on earthquake-fire coupling failure mechanism of steel cylindrical tanks. Reliability Engineering and System Safety 2024;245:110016. https://doi.org/10.1016/j.ress.2024.110016. 2024.
[14] Nikellis A, Sett K, Whittaker S. Multihazard Design and Cost-Benefit Analysis of Buildings with Special Moment-Resisting Steel Frames. J Struct Eng 2019;145(5):04019031. https://doi.org/10.1061/(ASCE)ST.1943-541X.0002298. 2019.
[15] Bi W, Tian L, Li C, Ma Z. A Kriging-based probabilistic framework for multi-hazard performance assessment of transmission tower-line systems under coupled wind and rain loads. Reliability Engineering and System Safety 2023;240:109615. https://doi.org/10.1016/j.ress.2023.109615. 2023.
[16] Barbato M, Petrini F, Unnikrishnan VU, Ciampoli M. Performance-Based Hurricane Engineering (PBHE) framework. Structural Safety 2013;45:24–35. https://doi.org/10.1016/j.strusafe.2013.07.002.
[17] Petrini F, Gkoumas K, Rossi C, Bontempi F. Multi-Hazard Assessment of Bridges in Case of Hazard Chain: State of Play and Application to Vehicle-Pier Collision Followed by Fire. Frontiers in Built Environment - Bridge Engineering 2020. https://doi.org/10.3389/fbuil.2020.580854. 15 September 2020.
[18] Goulet CA, Haselton CB, Mitrani-Reiser J, Beck JL, Deierlein GG, Porter KA, Stewart JP. Evaluation of the seismic performance of a code-conforming reinforced-concrete frame building—From seismic hazard to collapse safety and economic losses. Earthquake Engng Struct. Dyn. 2007;36:1973–97. https://doi.org/10.1002/eqe.694. 2007.
[19] Cornell AC, Jalayer F, Hamburger RO, Foutch DA. Probabilistic Basis for 2000 SAC Federal Emergency Management Agency Steel Moment Frame Guidelines. J Struct Eng 2002;128(4):526–33. https://doi.org/10.1061/(ASCE)0733-9445(2002)128:4(526).
[20] Jalayer F, Franchin P, Pinto PE. A scalar damage measure for seismic reliability analysis of RC frames. Earthquake Engng Struct. Dyn. 2009;36:2059–79. https://doi.org/10.1002/eqe.704. 2007.
[21] Petrini F, Francioli M. Next generation PBWE: Extension of the SAC-FEMA method to high-rise buildings under wind hazards. Structural Safety 2022;99:102255. https://doi.org/10.1016/j.strusafe.2022.102255. 2022.
[22] Vamvatsikos D. Accurate Application and Second-Order Improvement of SAC/FEMA Probabilistic Formats for Seismic Performance Assessment. J. Struct. Eng. 2014;140. https://doi.org/10.1061/(ASCE)ST.1943-541X.0000774. 2014.
[23] Franchin P, Pinto PE. Method for Probabilistic Displacement-Based Design of RC Structures. J. Struct. Eng. 2012;138:585–91. https://doi.org/10.1061/(ASCE)ST.1943-541X.0000492. 2012.
[24] Romão X, Delgado R, Costa A. Alternative closed-form solutions for the mean rate of exceedance of structural limit states. Earthquake Engng Struct. Dyn. 2013;42:1827–45. https://doi.org/10.1002/eqe.2300. 2013.
[25] Franchin P, Petrini F, Mollaioli F. Improved risk-targated performance-based seismic design of reinforced concrete frame structures. Earthquake Engng Struct Dyn 2018;47:49–67. https://doi.org/10.1002/eqe. 2018.
[26] Jalayer F, Ebrahimian H, Miano A. Intensity-based demand and capacity factor design: A visual format for safety checking. Earthquake Spectra 2020:1–24. https://doi.org/10.1177/8755293020919451.
[27] Sharma A, Mittal H, Gairola A. Mitigation of wind load on tall buildings through aerodynamic modifications. Review. J of Build Eng 2018;18:180–94. https://doi.org/10.1016/j.jobe.2018.03.005. 2018.
[28] Tamura T, Miyagi T, Kitagishi T. Numerical prediction of unsteady pressures on a square cylinder with various corner shapes. J Wind Eng Ind Aerodyn 1998;74:531–42. https://doi.org/10.1016/S0167-6105(98)00048-8. 1998.
[29] Li YG, Yan JH, Li Y, Xiao CX, JMa JX. Wind tunnel study of wind effects on 90° helical and square tall buildings: A comparative study. Journal of Building Engineering 2021;42:103068. https://doi.org/10.1016/j.jobe.2021.103068. 2021.
[30] Kwok KCS, Hitchcock PA, Burton MD. Perception of vibration and occupant comfort in wind-excited tall buildings. J Wind Eng Ind Aerodyn 2009;97(7–8):368–80. https://doi.org/10.1016/j.jweia.2009.05.006.
[31] Lamb S, Kwok KCS, Walton D. Occupant comfort in wind-excited tall buildings: Motion sickness, compensatory behaviours and complaint. J Wind Eng Ind Aerodyn 2013;119:1–12. https://doi.org/10.1016/j.jweia.2013.05.004.
[32] Architectural Institute of Japan (AIJ). Guidelines for the evaluation of habitability to building vibration. AIJ-GEH-2004, Maruzen, Tokyo. 2004.
[33] ISO 10137. Bases for Design of Structures – Serviceability of Buildings and Walkways Against Vibrations. Geneva (Switzerland), International Organization for Standardization. 2007.
[34] Solari G, Piccardo G. Probabilistic 3-D turbulence modeling for gust buffeting of structures. Probabilistic Engineering Mechanics 2001;16:73–86. https://doi.org/10.1016/S0266-8920(00)00010-2.
[35] Carassale L, Solari G. Monte Carlo simulation of wind velocity field on complex structures. Journal of Wind Engineering and Industrial Aerodynamics 2006;94(1):323–39. https://doi.org/10.1016/j.jweia.2006.01.004.
[36] Chuang Wei-Chu, Spence SMJ. A framework for the efficient reliability assessment of inelastic wind excited structures at dynamic shakedown. Journal of Wind Engineering and Industrial Aerodynamics 2022;220:104834. https://doi.org/10.1016/j.jweia.2021.104834. 2022ISSN 0167-6105.
[37] Zhou Y, Kijeswski T, Kareem A. Along-Wind Load Effects on Tall Buildings: Comparative Study of Major International Codes and Standards. Journal of Structural Engineering 2002;128(6). June 12002.
[38] Liang S, Liu S, Li QS, Zhang L, Gu M. Mathematical model of acrosswind dynamic loads on rectangular tall buildings. J. Wind Eng. Ind. Aerodyn. 2002;90(12–15):1757–70. https://doi.org/10.1016/S0167-6105(02)00285-4.
[39] ESDU (2001). Report N. 86010: Characteristic of atmospheric turbulence near the ground. Part III: variations in space and time for strong winds (neutral atmosphere), http://www.esdu.com.
[40] Soong TT, Grigoriu M. Random vibration of mechanical and structural systems. New Jersey: Prentice-Hall; 1993.
[41] Gurley KR, Tognarelli MA, Kareem A. Analysis and Simulation Tools For Wind Engineering. Prob. Engng Mech. Vol. 1997;12(1):9–31.

[42] Davenport AG. Note on the distribution of the largest value of a random function with application to gust loading. Proc. Institution of Civil Engineers London 1964; 28:187–96. 1964.
[43] Günay MS, Sucuoglu H. An improvement to linear-elastic procedures for seismic performance assessment. Earthq Eng Struct Dyn 2010;39(8):907–31. https://doi.org/10.1002/eqe.980. 2010.
[44] Moon KS. Developments of Structural Systems Toward Mile-High Towers. International Journal of High-Rise Buildings 2018;7(3):197–214. https://doi.org/10.21022/IJHRB.2018.7.3.197. September 2018.
[45] Brunesi E, Nascimbene R, Casagrande L. Seismic analysis of high-rise mega-braced frame-core buildings. Eng Struct 2016;115:1–17. https://doi.org/10.1016/j.engstruct.2016.02.019. 2016.
[46] Carpinteri A, Lacidogna G, Cammarano S. Structural analysis of high-rise buildings under horizontal loads: A study on the Intesa Sanpaolo Tower in Turin. Eng Struct 2013;56:1362–71. https://doi.org/10.1016/j.engstruct.2013.07.009. 2013.
[47] Petrini F, Ciampoli M. Performance-based wind design of tall buildings. Structure and Infrastructure Engineering: Maintenance, Management, Life-Cycle Design and Performance 2012;8(10):954–66. https://doi.org/10.1080/15732479.2011.574815.
[48] America Society for Civil Engineering, (ASCE) (2023), "Prestandard for Performance-Based Wind Design v1.1" Published by American Society of Civil Engineers 1801 Alexander Bell Drive Reston, Virginia 20191–4382.
[49] CNR (NATIONAL RESEARCH COUNCIL OF ITALY) 2008. Guide for the assessment of wind actions and effects on structures. Technical report CNR-DT 207/2008, Rome (ITALY).
[50] Kareem A, Kijewski T, Tamura Y. Mitigation of motions of tall buildings with specific examples of recent applications. Wind and Structures 1999;2(3):201–51. 1999.
[51] Kareem A, Gurley KR. Damping in structures: its evaluation and treatment of uncertainty. Journal of Wind Engineering and Industrial Aerodynamics 1996;59:131–57. 1996.
[52] Ciabattoni M, Petrini F, Pamapanin S. Multi-hazard design of low-damage high-rise steel–timber buildings subjected to wind and earthquake loading. Eng Struct 2023;303:117522. https://doi.org/10.1016/j.engstruct.2024.117522. 2024.
[53] Boggs, D., Dragovich, J. (2006). The Nature of Wind Loads and Dynamic Response. CPP online report SP-240—2. Available at ⟨https://www.cppwind.com/wp-content/uploads/2020/12/WindLoadsDynamicResponses-Boggs2006.pdf⟩ (accessed April, 9, 2021).